OPEN

Correspondence and
requests for materials
should be addressed to
X.H.C. (chenxh@ustc.
edu.cn)

Electronic and magnetic phase diagram in $K_xFe_{2-y}Se_2$ superconductors

Y. J. Yan[1], M. Zhang[1], A. F. Wang[1], J. J. Ying[1], Z. Y. Li[1], W. Qin[1], X. G. Luo[1], J. Q. Li[2], Jiangping Hu[2,3] & X. H. Chen[1]

[1]Hefei National Laboratory for Physical Sciences at Microscale and Department of Physics, University of Science and Technology of China, Hefei, Anhui 230026, China, [2]Beijing National Laboratory for condensed Matter Physics, Institute of Physics, Chinese Academy of Sciences, Beijing 100190, China, [3]Department of Phyiscs, Purdue University, West Lafayette, Indiana 47907, USA.

The correlation and competition between antiferromagnetism and superconductivity are one of the most fundamental issues in high temperature superconductors. Superconductivity in high temperature cuprate superconductors arises from suppressing an antiferromagnetic (AFM) Mott insulator[1] while in iron-pnictide superconductors arises from AFM semimetals and can coexist with AFM orders[2–9]. This difference raises many intriguing debates on the relation between the two classes of high temperature superconductors. Recently, superconductivity at 32 K has been reported in iron-chalcogenide superconductors $A_xFe_{2-y}Se_2$ (A=K, Rb, and Cs)[10–12]. They have the same structure as that of iron-pnictide 122-system[13–15]. Here, we report electronic and magnetic phase diagram of $K_xFe_{2-y}Se_2$ system as a function of Fe valence. We find a superconducting phase sandwiched between two AFM insulating phases. The two insulating phases are characterized by two distinct superstructures caused by Fe vacancy orders with modulation wave vectors of $q_1=(1/5, 3/5, 0)$ and $q_2=(1/4, 3/4, 0)$, respectively.

U nderstanding whether antiferromagnetism is responsible for superconductivity in high temperature superconductors continues to be one of the most important unresolved problems in modern condensed matter physics. The parent compounds of both iron-pnictide and curpate high temperature superconductors exhibit strong antiferromagnetism[1,5,6,16–18]. The parent compounds of iron-pnictide superconductors are semimetal and the superconductivity can coexist with AFM order[2–9], while AFM Mott-insulators for cuprates and the superconductivity is developed after the AFM order is completely suppressed by doping[1,16]. These critical differences have led to intensive debate whether the iron-pnictides are weakly coupled or strongly correlated electron systems. In the weak coupling approach, the AFM order in iron-pnictides is generated by the nesting between the electron-like Fermi surfaces near the zone corner and the hole-like Fermi surfaces near the zone center in the Brillouin zone. The scatterings between the hole and electron pockets have been shown to drive a $s^{\pm}$ pairing symmetry, a s-wave pairing symmetry characterized by opposite signs between the hole and electron Fermi surfaces[19–25]. In the strong coupling approach, the AFM order is mainly contributed from local spin moments and stabilized by the next nearest neighbor AFM exchange couplings between them. In the superconducting state, these AFM exchange couplings also drive the $s^{\pm}$ pairing symmetry[23,26].

The newly discovered iron chalcogenide superconductors $A_xFe_{2-y}Se_2$ conceptually challenge the weak coupling picture in iron-pnictides because only electron Fermi surfaces around the zone corners are observed so that the scattering between the hole and electron pockets can not be responsible for the superconductivity[27,28]. Moreover, the new materials display many intriguing physical properties: (i) They have strong insulating phase featured by eight orders of magnitude increase of resistance from high temperature to low temperature[10–12]; (ii) In contrast to the iron pnictides, they develop an AFM long-range order with Neel temperature (T_N) as high as 559 K and an ordered magnetic moment more than 3 μ_B[29]; (iii) they also display iron vacancy order at a temperature Ts=578 K, higher than T_N[29]. The insulating phase and the large magnetic moment imply that the physics in $A_xFe_{2-y}Se_2$ is rather local. However, we still lack of a systematic phase diagram of $K_xFe_{2-y}Se_2$ to manifest the correlation and competition between AFM and superconductivity because of the existence of intrinsic Fe vacancies. The Fe vacancy order[30,31] causes $A_xFe_{2-y}Se_2$ non-stoichiometric, so that the study on superconductivity and the determination of their parent compounds have been complicated and difficult.

Here, we report the electronic and magnetic phase diagram of $K_xFe_{2-y}Se_2$ system as a function of Fe valence (V_{Fe}). The Fe valence is systematically controlled by changing the x and y in $K_xFe_{2-y}Se_2$ system. By measuring the resistivity, magnetic susceptibility, Seebeck coefficient, and vacancy ordering pattern of tens of samples, we

determined that the phase diagram of $K_xFe_{2-y}Se_2$ system consists of three regions with distinct physical properties. We indentify that there exist two insulting phases with a gap larger than 0.3 eV, and the superconductivity occurs in a narrow region of the Fe valence from 2 to ~1.94 between the two insulating phases.

Results

Our main results are shown in Fig. 1a, which maps out the detailed electronic and magnetic phase diagram against V_{Fe}. V_{Fe}, ranging from 1.86 to 2.06, is obtained from tens of single crystals with nominal different compositions of $A_xFe_{2-y}Se_2$ (see Table I). First of all, all the samples behave as a paramagnetic weak metal above a certain temperature (T_S), at which a structural transition takes place due to the formation of the Fe vacancy order. Just slightly below T_S, an AFM transition happens at a temperature T_N. Below T_N, there are three distinct regions as a function of the Fe valence for all the samples. In the region I with $V_{Fe} \geq 2.00$, an insulating state with long range AFM order is observed. In the region II with $1.935 < V_{Fe} < 2.00$, a superconducting state is observed together with a long range AFM order. The superconducting transition temperature (T_C), around 30 K, is
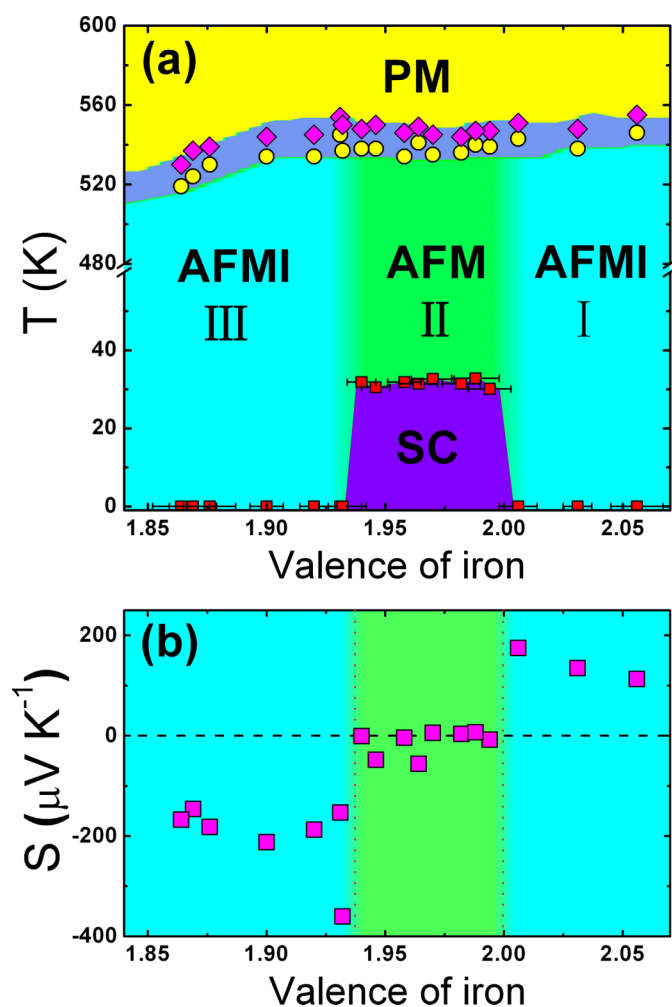
Figure 1 | Electronic and magnetic phase diagram of $K_xFe_{2-y}Se_2$ as a function of Fe valence. (a): The phase diagram plotted against the valence of iron. The Néel temperature (T_N) of the AFM transition determined by magnetic susceptibility (circles), the superconducting transition temperature (T_C) obtained by resistivity and susceptibility (squares), the temperature of the structural transition due to Fe vacancy ordering determined from the derivative of resistivity (diamonds); PM: paramagnetic metal; SC: superconducting state; AFMI: antiferromagnetic insulator; (b): Evolution of Seebeck coefficients at 300 K (squares) with the valence of iron.

robust against the Fe valence. In the region III with $V_{Fe} < 1.935$, another insulating state with a long range AFM order is formed. In the region I and II, the Ts and T_N are very robust against the Fe valence, while decrease obviously with reducing V_{Fe} in the region III.

We further confirm the phase diagram by measuring the Seebeck coefficients. The Seebeck coefficient at 300 K is plotted against the Fe valence in Fig. 1b for all the samples studied in phase diagram. The typical behavior of the Seebeck coefficients in the three regions is shown in Fig. 2, and the complete experimental data for all the samples are shown in Fig. S5 of supplementary information. As shown in Fig. 2, the Seebeck coefficient systematically changes with the Fe valence. The coefficients are large positive and large negative values in the two insulating phases $V_{Fe} > 2.00$ and $V_{Fe} < 1.935$, respectively. The result indicates the opposite types of the dominant charge carriers in the two insulating phases. In the region II, very small Seebeck coefficients were observed at 300 K. Such evolution of the Seebeck coefficients suggests the existence of Lifshitz transitions as the system moves into the superconducting region from the two insulating sides with a sudden change of the Fermi surface at the boundaries.

To understand the difference between two insulating phases, we use TEM to examine iron vacancy order in the region I and III. Fig. 3 shows the typical TEM observations on the single crystals in the three regions of phase diagram. Fig. 3a shows a high-resolution TEM image taken from thin crystal in the region I, in which the ordered behavior as visible periodic features within the **a–b** plane can be clearly read out. Superstructure spots with the main diffraction spots, which are originated from the Fe vacancy ordering, are observed. Fig. 3b shows the satellite spots in the **a*–b*** plane of reciprocal space in the region I. The spots are characterized by a unique modulation wave vector $q_1 = (1/5, 3/5, 0)$. Fig. 3c shows typical electron diffraction pattern taken along the [001] zone-axis directions in the region III, which exhibits the superstructure reflections in the **a*–b*** plane with a modulation wave vector $q_2 = (1/4, 3/4, 0)$. The small arrow indicates a $(1/2, 1/2, 0)$ spot which may be due to K order. These results definitely indicate two distinct insulating phases. To compare the superconducting phase with the insulating phases, we show the high-resolution TEM images taken from the insulating crystal $K_{0.79}Fe_{1.60}Se_2$ in the region I (shown in Fig. 3d) and the superconducting crystal $K_{0.73}Fe_{1.68}Se_2$ in region II (shown in Fig. 3e). The insulating sample shows a homogeneous phase with Fe vacancy order. However, the superconducting crystal exhibits two phases: the image in some areas is the same as that observed in the insulating sample with Fe vacancy order, while in other areas, the image is totally different and no Fe vacancy is found. It is worth noting that the observation in Fig. 3e is a common feature for all superconducting samples. These results conclude that the superconductivity occurs in the phase without Fe vacancy and the phase separation between the two phases takes place in superconducting crystals. This conclusion is consistent with two sets of c-axis lattice constant shown in the inset of Fig. 4d. The composition analysis listed in Table I also supports it: the average Fe content for all superconducting samples is around 1.66, while for all the insulating samples in the region I and III is around 1.61. The phase separation in the superconducting samples also offers a natural explanation about the little variation of T_N and T_S as a function of the Fe valence since T_N and T_S are determined by the insulating phase. It has been controversial whether the AFM and superconducting orders coexist microscopically[32,33] or the two are phase-separated[33,35]. Our results here clearly support that the latter is the case. In addition, there exist two Fe vacancy ordering with wave vector of $(1/5, 3/5, 0)$ and $(1/4, 3/4, 0)$ in the superconducting samples due to the phase separation of insulating phases and superconducting phase[35].

Discussion

Finally, we discuss the correlation between the structural, compositional, and electronic properties characteristic for the three phases of

Table I | The nominal and actual compositions, onset temperature of superconducting transition (T_C), AFM transition temperature (T_N), structure transition temperature (T_S) and Seebeck coefficient at 300 K ($S_{300 K}$) for the $K_xFe_{2-y}Se_2$ single crystals

| Nominal composition	Actual composition	Valence of iron	T_c (K)	T_N (K)	T_S (K)	S_{300K} ($\mu V/K$)
$KFe_{1.5}Se_2$	$K_{0.989\pm0.017}Fe_{1.611\pm0.009}Se_2$	1.869 ± 0.010	0	524	537	-146
$KFe_{1.55}Se_2$	$K_{0.978\pm0.016}Fe_{1.621\pm0.012}Se_2$	1.864 ± 0.012	0	519	530	-167
KFe_2Se_2	$K_{0.980\pm0.017}Fe_{1.610\pm0.009}Se_2$	1.876 ± 0.011	0	530	539	-182
$KFe_{2.4}Se_2$	$K_{0.963\pm0.011}Fe_{1.598\pm0.015}Se_2$	1.900 ± 0.007	0	534	544	-212
$K_{0.9}Fe_{1.5}Se_2$	$K_{0.910\pm0.015}Fe_{1.600\pm0.014}Se_2$	1.931 ± 0.009	0	545	554	-153
$K_{0.9}Fe_{1.55}Se_2$	$K_{0.892\pm0.010}Fe_{1.619\pm0.005}Se_2$	1.920 ± 0.006	0	534	545	-187
$K_{0.9}Fe_{1.7}Se_2$	$K_{0.888\pm0.016}Fe_{1.611\pm0.008}Se_2$	1.932 ± 0.010	0	537	550	-360
$K_{0.8}Fe_{1.7}Se_2$	$K_{0.763\pm0.013}Fe_{1.648\pm0.013}Se_2$	1.964 ± 0.008	31.4	541	549	-56
$K_{0.8}Fe_{1.75}Se_2$	$K_{0.734\pm0.011}Fe_{1.678\pm0.006}Se_2$	1.946 ± 0.006	30.5	538	550	-48
$K_{0.8}Fe_{1.8}Se_2$	$K_{0.711\pm0.015}Fe_{1.649\pm0.015}Se_2$	1.994 ± 0.009	30.1	539	547	-7.7
$K_{0.8}Fe_2Se_2$	$K_{0.733\pm0.012}Fe_{1.668\pm0.012}Se_2$	1.958 ± 0.007	31.8	534	546	-4.0
$K_{0.8}Fe_{2.2}Se_2$	$K_{0.759\pm0.010}Fe_{1.671\pm0.008}Se_2$	1.940 ± 0.006	31.8	538	548	-0.5
$K_{0.8}Fe_{2.4}Se_2$	$K_{0.730\pm0.013}Fe_{1.650\pm0.013}Se_2$	1.982 ± 0.008	31.4	536	544	3.4
$K_{0.8}Fe_{2.6}Se_2$	$K_{0.758\pm0.016}Fe_{1.631\pm0.017}Se_2$	1.988 ± 0.010	32.8	540	547	7.0
$K_{0.8}Fe_3Se_2$	$K_{0.727\pm0.015}Fe_{1.661\pm0.007}Se_2$	1.970 ± 0.009	32.6	535	545	5.7
$K_{0.8}Fe_{1.6}Se_2$	$K_{0.792\pm0.013}Fe_{1.599\pm0.014}Se_2$	2.006 ± 0.008	0	543	551	175
$K_{0.75}Fe_{1.6}Se_2$	$K_{0.754\pm0.010}Fe_{1.598\pm0.008}Se_2$	2.031 ± 0.006	0	538	548	135
$K_{0.7}Fe_{1.65}Se_2$	$K_{0.687\pm0.017}Fe_{1.611\pm0.011}Se_2$	2.056 ± 0.011	0	546	555	113

$A_xFe_{2-y}Se_2$ system. We study the physical properties for the samples with nominal compositions $A_{1-x}Fe_{1.5+x/2}Se_2$ (x=0, 0.1, 0.2, and 0.3) to keep the nominal valence of Fe to be +2. As shown in Fig. 4a, all these crystals show insulating behavior with activation energy of about 100 meV. Resistivity exhibits a rapid increase around 550 K, and a subsequent insulating behavior to the low temperature. The resistivity increases by about eight orders of magnitude as the temperature decreases from 500 K to 60 K. No superconductivity can be observed for this series of samples. Composition analysis indicates that the actual K contents are nearly the same as the nominal compositions, while the actual Fe contents are around 1.60 for all the crystals. This indicates that the insulating phase is closely related to Fe content, while has nothing to do with K content. Meanwhile, the value of Seebeck coefficient at 300 K is negative for the samples with higher K content in region III, while positive for the samples with lower K content in region I, which is one of the direct experimental evidences to distinguish the two insulating phases. Therefore, the K

content is very important for the physical properties of $A_xFe_{2-y}Se_2$. To further determine the influence of K and Fe content on electronic properties, we focus on the two series of samples $A_xFe_ySe_2$ with K content of 0.8 and 1, respectively. Figure 4b shows the resistivity as a function of temperature in KFe_ySe_2 system. All the samples show insulating behavior and no trace for superconductivity can be found. A sharp rapid increase in resistivity takes place at the temperature ranging from 525 K to 550 K due to the Fe vacancy and AFM ordering. The elemental analysis (as shown in Table I) indicates that the actual K concentration for all the samples is nearly 1, being the same as nominal composition. It is amazing that the actual Fe content is around 1.6, and does not change with increasing Fe content in starting materials. Therefore, the Fe valence keeps less than 1.94 for the crystals with K content around 1, so that these samples always fall in the region III of the phase diagram. Much more Fe vacancies are expected because the ionic state with much less than +2 is not stable. This offers an explanation why the superconductivity cannot occur in the samples with K content of 1 in the $KFe_{2-y}Se_2$ system. These results suggest that Fe vacancy arises from charge balance and is bad to superconductivity. Moreover, K content is very important for superconductivity. Figure 4c shows the in-plane resistivity for the crystals of $K_{0.8}Fe_{1.6+y}Se_2$ ($y \geq 0.1$). All the samples show similar resistivity behavior. At the temperature around 550 K, the resistivity shows a rapid increase and subsequently semiconductor-like behavior with decreasing temperature. As the temperature decreases further, the resistivity exhibits metallic behavior, and the superconductivity develops around 30 K although the samples still show an AFM transition above 500 K (see supplementary information) as well as large resistivity in the normal state. A fully superconducting shielding volume fraction is observed by susceptibility in Fig. 4d. It is found that the samples with nominal composition $K_{0.8}Fe_{1.6+y}Se_2$ falls in the region I of phase diagram for y<0.1, while in the region II of phase diagram for $y \geq 0.1$. The elemental analysis (as shown in Table I) shows that all the samples in region II of phase diagram have a higher actual Fe content of about 1.63 to 1.67 with a lower K content of about 0.74, leading to a Fe valence between 1.94 and 2.0. But for $K_{0.8}Fe_{1.6+y}Se_2$ (y<0.1) which is an insulator in region I of phase diagram, the actual Fe content keeps around 1.61. In summary, the K and Fe contents have great influence on the structural and physical properties of $A_xFe_{2-y}Se_2$ system. The superconducting phase II has a higher Fe content of about 1.63 to 1.67 with a lower K content of about 0.74, while the two insulating phases have a lower Fe content of about 1.61. Meanwhile, negative Seebeck coefficient
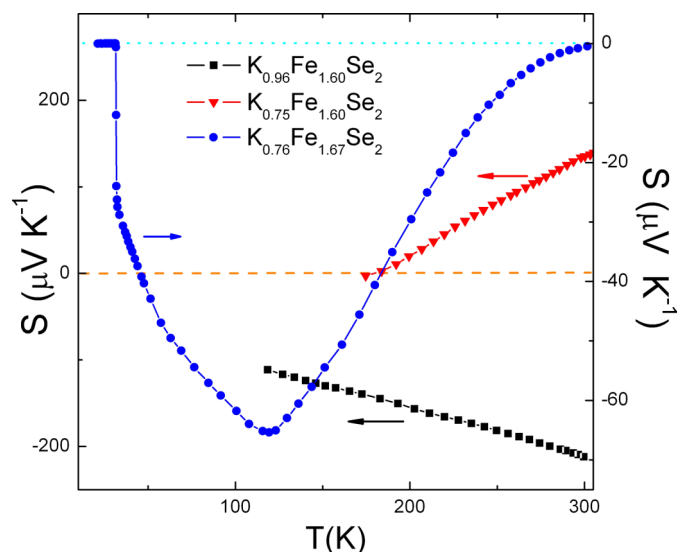
Figure 2 | Typical Seebeck coefficient as a function of temperature for the samples in the three regions of the phase diagram. Region I: $K_{0.75}Fe_{1.6}Se_2$; Region II: $K_{0.76}Fe_{1.67}Se_2$; Region III: $K_{0.96}Fe_{1.60}Se_2$.
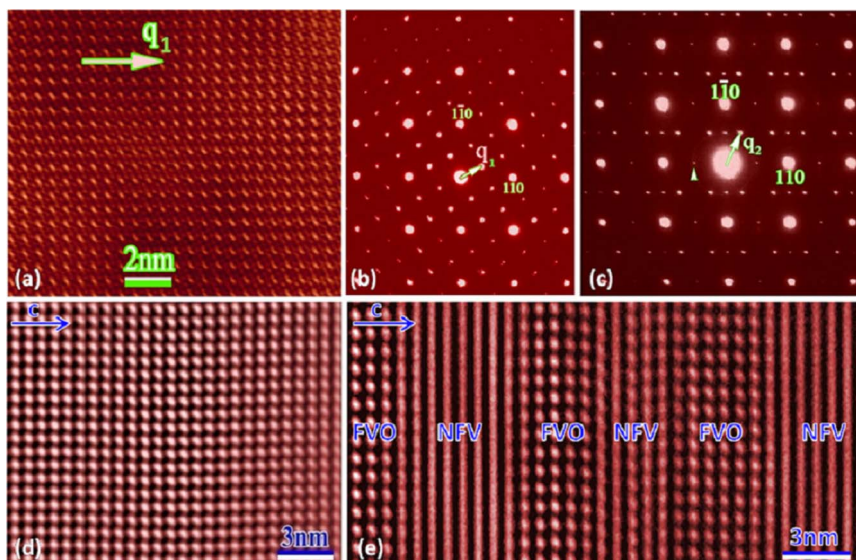
Figure 3 | High-resolution TEM images and electron diffraction patterns for the samples in the two insulating phases and superconducting phase. (a): High-resolution TEM image of $K_{0.79}Fe_{1.6}Se_2$ in the region I taken along the [001] zone-axis direction, in which the ordered behavior as visible periodic features within the a–b plane can be clearly read out; (b): Electron diffraction pattern of $K_{0.79}Fe_{1.6}Se_2$ in the region I taken along the [001] zone-axis direction, superstructure spots are clearly visible in the a^*–b^* plane of reciprocal space and can be characterized by a unique modulation wave vector $q_1 = (1/5, 3/5, 0)$; (c): Electron diffraction pattern of $K_{0.99}Fe_{1.61}Se_2$ in the region III taken along the [001] zone-axis direction, showing the superstructure reflections within the a–b reciprocal plane with wave vector $q_2 = (1/4, 3/4, 0)$, and small arrow indicates $(1/2, 1/2, 0)$ spots; (d): High-resolution TEM image of the insulating crystal $K_{0.79}Fe_{1.60}Se_2$ in the region I taken along c-axis direction, in which the ordered behavior as visible periodic features along c-axis direction can be clearly read out. (e): High-resolution TEM image of the superconducting crystal $K_{0.73}Fe_{1.68}Se_2$ in the region II taken along c-axis direction. The image in some areas is the same as that observed in Fig. 3d for insulating sample, in which Fe vacancy order (FVO) occurs. In other areas, the image is totally different from that with Fe vacancy order, and no Fe vacancy (NFV) is found in these areas. It indicates the phase separation in the superconducting sample.
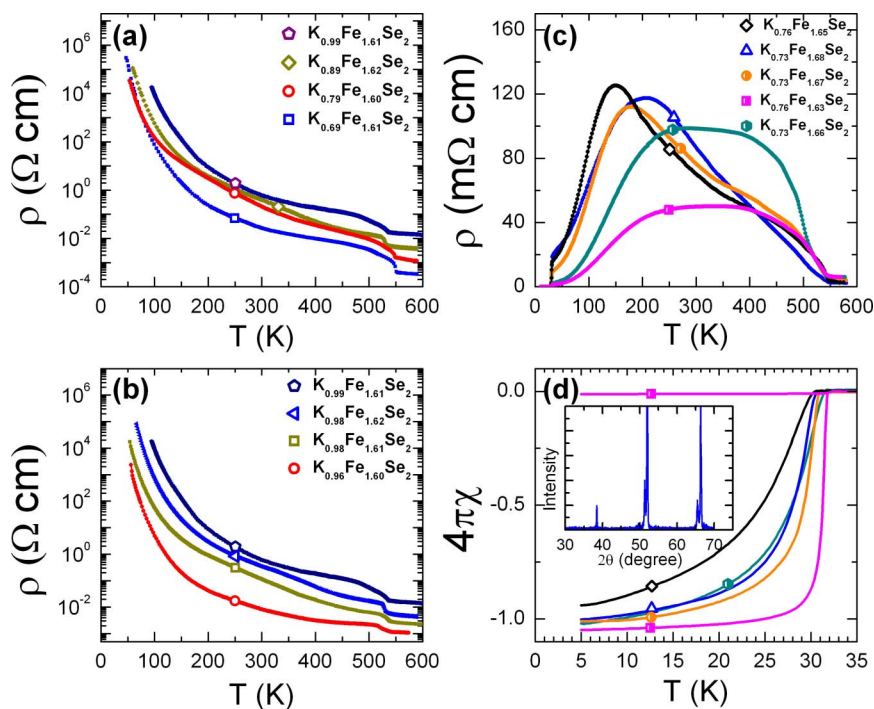
Figure 4 | Evolution of transport properties and superconductivity from region I to region III in the phase diagram. The actual compositions were given in Figure. (a): Temperature dependence of the in-plane resistivity for the insulating samples with the nominal composition of $K_{1-x}Fe_{1.5+x/2}Se_2$ ($x=0, 0.1, 0.2, 0.3$); (b): In-plane resistivity as a function of temperature for the insulating crystals with nominal composition of $KFe_{1.5+y}Se_2$ ($y = 0, 0.05, 0.5, 0.9$) in the region III; (c): Temperature dependence of the resistivity for the crystals grown with the nominal composition of $K_{0.8}Fe_{1.6+y}Se_2$ ($0.1 \leq y \leq 1.4$) in region II. (d): The magnetic susceptibility data measured with a zero-field-cooling (ZFC) process and a field of 10 Oe applied within the ab-plane for the same crystals as that measured in (c). The field-cooling (FC) susceptibility with magnetic field of 10 Oe applied with the ab-plane fails to show Meissner effect for the $K_{0.76}Fe_{1.63}Se_2$ crystal. The inset of (d) shows the reflections of single crystal XRD taken at 300 K for $K_{0.73}Fe_{1.67}Se_2$ crystal, and two sets of reflections are observed, suggesting an intergrowth behavior and two phases in superconducting crystal. This is consistent with the TEM observation shown in Fig. 3e.

at 300 K was observed in phase III with higher K content, while positive value in phase I with lower K content.

In summary, we determine the electronic and magnetic phase diagram of $A_xFe_{2-y}Se_2$ and show that the K and Fe contents have great influence on the structural and physical properties of $A_xFe_{2-y}Se_2$ system. The superconducting phase II has a higher Fe content of about 1.63 to 1.67 with a lower K content of about 0.74, while the two insulating phases have a lower Fe content of about 1.61. Negative Seebeck coefficient at 300 K was observed in phase III with higher K content, while positive value in phase I with lower K content. The insulating phase in the region III could arise from the Fe vacancy order. AFM and superconducting orders are phase-separated in the samples of region II. Our findings cast new insight on the origin and mechanism of superconductivity in iron-based superconductors.

Methods

$K_xFe_ySe_2$ single crystals used in this study were grown by using Bridgman method[11]. The compositions of crystals were determined using an energy-dispersive X-ray spectrometer (EDS) mounted on the field emission scanning electronic microscope (FESEM), Sirion200. At least five spots for each crystal have been measured to obtain the average potassium and iron concentration by considering selenium as 2. To make sure that the obtained compositions from EDS are consistent with each batch, more than two pieces of crystal for each sample from the same batch were used to determine the composition. We measured the composition on the different spots of the each piece, and found the composition determined from the different spots is nearly the same within the error bars, suggesting the samples are homogeneous. The average valence of iron was obtained for each crystal by calculation with formula: $(4-x)/y$ assuming without Se vacancy, where x and y were the actual concentration of potassium and iron from elemental analysis. All these results have been listed in Table I. The errors of the actual components and the valence of iron are obtained by standard deviation calculation with three significant digits after the decimal point listed in Table I. But we used two significant digits after the decimal point in the text and figures when describing the actual components of the samples for simplicity. We measured resistivity using standard four-probe method. For resistivity below 400 K, the measurements were carried out by using *Quantum Design* PPMS-9. The measurement of high temperature resistivity above 300 K was performed by using LR700 alternative current Resistance bridge with Type-K Chromel-Alumel thermocouples as thermometer in a home-built high-temperature oven. Magnetic susceptibility was measured by using *Quantum Design* MVSM-MPMS. High-temperature magnetic susceptibility was measured using high-temperature oven in a *Quantum Design* SQUID-MPMS-7. The Seebeck coefficients were measured on *Quantum Design* PPMS-9 with steady-state method by means of heat off and on mode. Specimens for TEM observation were prepared by peeling off a very thin sheet of a thickness around several tens microns from the single crystal and then milling by Ar ion. Microstructure analyses were performed on a FEI Tecnai-F20 TEM equipped with double-tilt cooling holder. Specific heat measurement was carried out on *Quantum Design* PPMS-9.

1. Lee, P. A., Nagaosa, N. & Wen, X.-G. Doping a Mott insulator: Physics of high-temperature superconductivity. *Rev. Mod. Phys.* **78**, 17–85 (2006).
2. Kamihara, Y., Watanabe, T., Hirano, M. & Hosono, H. Iron-basedlayered superconductor La[O$_{1-x}$F$_x$]FeAs (x = 0.05–0.12) with T$_c$ = 26 K. *J. Am. Chem. Soc.* **130**, 3296–3297 (2008).
3. Chen, X. H. *et al.* Superconductivity at 43 K in SmFeAsO$_{1-x}$F$_x$. *Nature* **453**,761–762 (2008).
4. Chen, H. *et al.* Coexistence of the spin-density wave and superconductivity in Ba$_{1-x}$K$_x$Fe$_2$As$_2$. *Europhys. Lett.* **85**, 17006 (2009).
5. Drew, A. J. *et al.* Coexistence of static magnetism and superconductivity in SmFeAsO$_{1-x}$F$_x$ as revealed by muon spin rotation. *Nature Mater* **8**, 310–314 (2009).
6. Johnston, D. C. The puzzle of high temperature superconductivity in layered iron pnictides and chalcogenides. *Adv. in Phys.* **59**, 803 (2010).
7. Medvedev, S. *et al.* Electronic and magnetic phase diagram of β-Fe$_{1.01}$Se with superconductivity at 36.7 K under pressure. *Nature Materials* **8**, 630–633 (2009).
8. Liu, T. J. *et al.* From (π, 0) magnetic order to superconductivity with (π, π) magnetic resonance in Fe$_{1.02}$Te$_{1-x}$Se$_x$. *Nature Materials* **9**, 716–720 (2010).
9. Nandi, S. *et al.* Anomalous Suppression of the Orthorhombic Lattice Distortion in Superconducting Ba(Fe$_{1-x}$Co$_x$)$_2$As$_2$ Single Crystals. *Phys. Rev. Lett.* **104**, 057006 (2010).
10. Guo, J. *et al.* Superconductivity in the iron selenide K$_x$Fe$_2$Se$_2$(0≤x≤1.0). *Phys. Rev. B* **82**, 180520 (2010).
11. Wang, A. F. *et al.* Superconductivity at 32 K in single-crystalline Rb$_x$Fe$_2$-$_y$Se$_2$. *Phys. Rev. B* **83**, 060512 (2011).
12. Krzton-Maziopa, A. *et al.* Synthesis and crystal growth of Cs$_{0.8}$(FeSe$_{0.98}$)$_2$: A new iron-based superconductor with T$_c$ = 27 K. *J. Phys. Condens. Matter* **23**, 052203 (2011).
13. Rotter, M., Tegel, M. & Johrendt, D. Superconductivity at 38 K in the iron arsenide (Ba$_{1-x}$K$_x$)Fe$_2$As$_2$. *Phys. Rev. Lett.* **101**, 107006 (2008).
14. Sasmal, K. *et al.* Superconducting Fe-Based Compounds (A$_{1-x}$Sr$_x$)Fe$_2$As$_2$ with A=K and Cs with Transition Temperatures up to 37 K. *Phys. Rev. Lett.* **101**, 107007 (2008).
15. Wu, G. *et al.* Different resistivity response to spin density wave and superconductivity at 20 K in Ca$_{1-x}$Na$_x$Fe$_2$As$_2$. *J. Phys. Condens. Matter* **20**, 422201 (2008).
16. Niedermayer, Ch. *et al.* Common phase diagram for antiferromagnetism in La$_{2-x}$Sr$_x$CuO$_4$ and Y$_{1-x}$Ca$_x$Ba$_2$Cu$_3$O$_6$ as seen by muon spin rotation. *Phys. Rev. Lett.* **80**, 3843–3846 (1998).
17. De la Cruz, C. *et al.* Magnetic order close to superconductivity in the iron-based layered LaO$_{1-x}$F$_x$FeAs system. *Nature* **453**, 899–902 (2008).
18. Huang, Q. *et al.* Neutron-diffraction measurements of magnetic order and a structural transition in the parent BaFe$_2$As$_2$ compound of FeAS-based high-temperature superconductors. *Phys. Rev. Lett.* **101**, 257003 (2008).
19. Ding, H. *et al.* Observation of Fermi-surface-independent nodeless superconducting gaps in Ba$_{0.6}$K$_{0.4}$Fe$_2$As$_2$. *Europhys. Lett.* **83**, 47001 (2008).
20. Christianson, A. D. *et al.* Unconventional superconductivity in Ba$_{0.6}$K$_{0.4}$Fe$_2$As$_2$ from inelastic neutron scattering. *Nature* **456**, 930–962 (2008).
21. Mazin, I. I. *et al.* Unconventional superconductivity with sign reversal in the ordered parameter of LaFeAsO$_{1-x}$F$_x$. *Phys. Rev. Lett.* **101**, 057003 (2008).
22. Kuroki, K. *et al.* Unconventional pairing originating from the disconnected Fermi surfaces of superconducting LaFeAsO$_{1-x}$F$_x$. *Phys. Rev. Lett.* **101**, 087004 (2008).
23. Seo, K., Bernevig, B. A. & Hu, J. P. Pairing symmetry in a two-orbital exchange coupling model of oxypnictides. *Phys. Rev. Lett.* **101**, 206404 (2008).
24. Wang, F. *et al.* A functional renormalization group study of the pairing symmetry and pairing mechanism of the FeAs based high temperature superconductors. *Phys. Rev. Lett.* **102**, 047005 (2009).
25. Si, Q. & Abrahams, E., Strong correlations and magnetic frustration in the high Tc iron Pnictides. *Phys. Rev. Lett* **101**, 076401 (2008).
26. Berg, E., Kivelson, S. A. & Scalapino, D. J. A twisted Ladder: Relating the iron superconductors and the high T$_C$ cuprates. *Phys. Rev. B* **81**, 172504 (2010).
27. Zhang, Y. *et al.* Nodeless superconducting gap in A$_x$Fe$_2$Se$_2$(A=K, Cs) revealed by angle-resolved photoemission spectroscopy. *Nature Materials* **10**, 273–277 (2011).
28. Qian, T. *et al.* Absence of holelike Fermi surface in superconducting K$_{0.8}$Fe$_{1.7}$Se$_2$ revealed by ARPES. *Phys. Rev. Lett* **106**, 187001 (2011).
29. Bao, W. *et al.* A Novel Large Moment Antiferromagnetic Order in K$_{0.8}$Fe$_{1.6}$Se$_2$ Superconductor. *Chinese Phys. Lett.* **28**, 086104 (2011).
30. Bacsa, J. *et al.* Cation Vacancy order in the K$_{0.8+x}$Fe$_{1.6-y}$Se$_2$ system: Five-fold cell expansion accommodates 20% tetrahedral vacancies. *Chem. Sci.* **2**, 1054–1058 (2011).
31. Zavalij, P. *et al.* On the Structure of Vacancy Ordered Superconducting Alkali Metal Iron Selenide. *Phys. Rev. B* **83**, 132509 (2011).
32. Shermadini, Z. *et al.* Coexistence of Magnetism and Superconductivity in the Iron-Based Compound Cs$_{0.8}$(FeSe$_{0.98}$)$_2$. *Phys. Rev. Lett.* **106**, 117602 (2011).
33. Liu, R. H. *et al.* Coexistence of superconductivity and antiferromagnetism in single crystals A$_{0.8}$Fe$_{2-y}$Se$_2$ (A = K, Rb, Cs, Tl/K and Tl/Rb): evidence from magnetization and resistivity. *Europhysics Letters* **94**, 27008 (2011).
34. Luo, X. G. *et al.* Crystal structure, physical properties and superconductivity in A$_x$Fe$_2$Se$_2$ single crystals. *New J. Phys.* **13**, (2011) 053011.
35. Wang, Z. *et al.* Microstructure and Fe-vacancy ordering in the KFe$_x$Se$_2$ superconducting system. *Phys. Rev. B* **83**, 140505 (2011).

Author contributions

Single crystals of A$_x$Fe$_{2-y}$Se$_2$ were grown by M.Z., A.F.W., Z.Y.L. and W. Q. Resistivity and magnetic susceptibility measurements were done by M.Z., A.F.W., W.Q., Y.J.Y. and J.J.Y. Seebeck coefficient was measured by Y.J.Y. XRD and element analysis measurements were carried out by M.Z., and A.F.W. J.Q.L. did TEM measurement. X.G.L., Y.J.Y., J.J.Y. and X.H.C analysed all the data. J.P.H. and X.H.C. wrote the paper. X.H.C. was responsible for project direction, planning and infrastructure.

Additional information

Supplementary information accompanies this paper at http://www.nature.com/scientificreports

Competing financial interests: The authors declare no competing financial interests.

How to cite this article: Yan, Y.J. *et al.* Electronic and magnetic phase diagram in K$_x$Fe$_{2-y}$Se$_2$ superconductors. *Sci. Rep.* **2**, 212; DOI:10.1038/srep00212 (2012).